

Contributions of the Large-Scale Environment to the Typhoon Genesis of Faxai (2019)

Hironori FUDEYASU

*Graduate School of Education, Yokohama National University, Yokohama, Japan
Typhoon Science and Technology Research Center, Yokohama National University, Yokohama, Japan*

Udai SHIMADA

*Meteorological Research Institute, Japan Meteorological Agency, Tsukuba, Japan
Typhoon Science and Technology Research Center, Yokohama National University, Yokohama, Japan*

Yoshinori OIKAWA

Japan Meteorological Agency, Tokyo, Japan

Hisaki EITO, Akiyoshi WADA

Meteorological Research Institute, Japan Meteorological Agency, Tsukuba, Japan

Ryuji YOSHIDA¹

*CIRES, University of Colorado Boulder, Colorado, USA
NOAA Earth System Research Laboratory, Colorado, USA
RIKEN Center for Computational Science, Kobe, Japan
Research Center for Urban Safety and Security, Kobe University, Kobe, Japan*

and

Takeshi HORINOUCHI

*Faculty of Environmental Earth Science, Hokkaido University, Sapporo, Japan
Typhoon Science and Technology Research Center, Yokohama National University, Yokohama, Japan*

(Manuscript received 21 April 2021, in final form 8 March 2022)

Abstract

This study investigated the atmospheric and oceanic contributions to the genesis of Typhoon Faxai in 2019. Our statistical analysis using the tropical cyclone genesis score (TGS) attributed the tropical disturbance that developed into Faxai (Pre-Faxai) to easterly waves (EWs). The EW score evaluated by a grid version of the TGS (Grid-EW) averaged around the occurrence of Pre-Faxai was approximately twice as large as the climatological mean, and it was the second largest value in the past 38 years. The Pre-Faxai area with high Grid-EW scores

Corresponding author: Hironori Fudeyasu, Faculty of Education, Yokohama National University, 79-2 Tokiwadai, Hodogaya-ku, Yokohama, 240-8501, Japan

E-mail: fude@ynu.ac.jp

¹ Present affiliation: Yokohama National University, Yokohama, Japan

J-stage Advance Published Date: 21 April 2022



could be traced back to the eastern North Pacific (ENP) around August 25, 2019. The lower-troposphere environment characterized by high Grid-EW scores was favorable for vortex formation because it provided a containment area for moisture entrained by the developing circulation or lofted by the deep convection therein. The Pre-Faxai area with high Grid-EW scores moved westward due to the background easterly flow over the ENP and then entered the western North Pacific (WNP). The Typhoon Intensity Forecast Scheme (TIFS) showed that the important environments for its genesis were ocean conditions and the vertical wind shear. The oceanic conditions contributed to the development of Pre-Faxai as it traveled over the WNP. The enhancement of vertical wind shear and subsequent suppression of the development of Pre-Faxai were caused by the lower-troposphere easterly winds associated with high EW scores. They were also caused by upper-troposphere westerly winds associated with an upper cold low northwest of Pre-Faxai. When the vertical shear decreased with weakening of the upper cold low, Pre-Faxai reached tropical storm intensity on September 4. Therefore, TGS and TIFS detected Pre-Faxai 10 days before the typhoon arose, which indicates that monitoring environmental factors such as EW and vertical wind shear are important for disaster prevention.

Keywords typhoon genesis; easterly waves; vertical wind shear; upper cold low

Citation Fudeyasu, H., U. Shimada, Y. Oikawa, H. Eito, A. Wada, R. Yoshida, and T. Horinouchi, 2022: Contributions of the large-scale environment to the typhoon genesis of Faxai (2019). *J. Meteor. Soc. Japan*, **100**, 617–630, doi:10.2151/jmsj.2022-031.

1. Introduction

Typhoon Faxai made landfall in Chiba, Japan, at 21 UTC September 8, 2019, causing enormous damage to the Kanto region. The winds were the strongest ever recorded in Japan, with instantaneous wind speeds of 57.5 m s^{-1} in Chiba City. According to the best-track (BT) data of the Regional Specialized Meteorological Center Tokyo–Typhoon Center, Faxai first reached tropical storm intensity (maximum sustained wind speeds greater than 17 m s^{-1}) at 18 UTC September 4, 2019. We refer to this as the typhoon genesis in this study. There were only 4 days for notification prior to landfall after typhoon genesis (Fig. 1). However, tropical cyclones (TCs) are generally first observed as tropical disturbances or lows several days before the typhoon genesis stage, which is defined as the period from the appearance of a tropical disturbance to the typhoon genesis itself.

The Japan Meteorological Agency (JMA) estimates the intensity and position of typhoons over the ocean mainly using the Dvorak method (Dvorak 1984), based on an analysis of Japanese Geostationary Meteorological Satellite cloud images. Because the organization period of clouds associated with a tropical disturbance during the genesis stage is short, the data are insufficient for analysis purposes. The Dvorak method is applied only a few days before the typhoon genesis. Therefore, the JMA has developed what has been referred to as “Early Dvorak Analysis” (EDA) to determine the position of tropical disturbance objectively

based on Geostationary Meteorological Satellite cloud images (Tsuchiya et al. 2001). Improvements to the EDA (Kishimoto et al. 2007; Kishimoto 2009) have allowed its use in forecasting operations since 2007.

According to the EDA, the tropical disturbance that developed into Typhoon Faxai (hereafter, Pre-Faxai) was first detected over the eastern North Pacific (ENP), immediately east of the International Date Line, at 12 UTC August 29, 2019 (Fig. 1). The genesis stage of Faxai, from the first detection of Pre-Faxai to typhoon genesis, lasted 6 days. The average duration of the TC genesis stage is 1.4 days, and only 3 % of all cases exceed 6 days, according to Fudeyasu et al. (2020) who analyzed the genesis stages of 476 TCs (including cases that dissipated before reaching tropical storm intensity) using EDA data for the period 2009–2017. In comparison, Pre-Faxai had an unusually long genesis stage, which was affected by the surrounding environment.

Ritchie and Holland (1999) examined large-scale flow patterns as the environmental factor contributing to typhoon genesis over the western North Pacific (WNP), i.e., the shear line, confluence region, monsoon gyre, easterly waves (EWs), and Rossby wave energy dispersion from a preexisting TC. The shear line and confluence region are enhanced by the easterly trade winds and westerly winds over the WNP. Typhoon genesis in the monsoon shear line occurs when the disturbance is located in a region of low mean sea-level pressure (Chen and Weng 1998). The confluence region between easterly and westerly

flows contains a range of scale interactions that can contribute to enhanced typhoon genesis conditions (Zhang and Webster 1989; Chang and Webster 1990). The monsoon gyre is a synoptic-scale gyre embedded within a developed Asian monsoon trough (Lander 1994; Chen et al. 1996). EWs occur in synoptic-scale easterly trade winds, with the trough of EWs providing an environment that is favorable for the genesis of a tropical disturbance (Heta 1990, 1991). A mature typhoon disperses its energy as a Rossby wave in a southeastward direction, and low-pressure areas of the wave train sometimes develop into another typhoon (McDonald 1998; Li and Fu 2006; Li et al. 2006). Yoshida and Ishikawa (2013) developed a TC genesis score (TGS) as an objective index to determine the contribution of five environmental factors to the occurrence of a tropical disturbance. This study used the TGS to identify the main environmental factors contributing to the occurrence of Pre-Faxai.

Furthermore, the developments in the main environmental factor of Pre-Faxai were investigated using a gridded TGS (Grid-TGS). Yoshida and Fudeyasu (2020) developed the Grid-TGS, which obtains the grid point values of five selected environmental factors. It is possible to investigate the temporal and spatial changes in each environmental factor, namely, the preconditioning of the environment leading to typhoon genesis. A detailed understanding of the preconditioning for typhoon genesis is important for disaster prevention and predictions of typhoon genesis.

This study also used the Typhoon Intensity Forecast Scheme (TIFS) based on the statistical hurricane intensity prediction scheme (Yamaguchi et al. 2018; Shimada et al. 2018) to assess the environmental contributions to the development of Pre-Faxai's intensity during the genesis stage. The statistical hurricane intensity prediction scheme is a statistical model that predicts the changes in intensity of hurricanes following the initial prediction using a multiple linear regression equation (DeMaria and Kaplan 1994, 1999; DeMaria et al. 2005). The advantage of the statistical hurricane intensity prediction scheme for typhoon intensity prediction is that the contribution of each predictor variable to the total intensity change can be quantified.

This study aimed to investigate the environmental factors responsible for the occurrence of Pre-Faxai, using the TGS and reanalysis data. Furthermore, the contribution of the surrounding environment to the genesis of Typhoon Faxai was quantitatively determined using the TIFS. The rest of this paper is organized as follows. Section 2 introduces the meth-

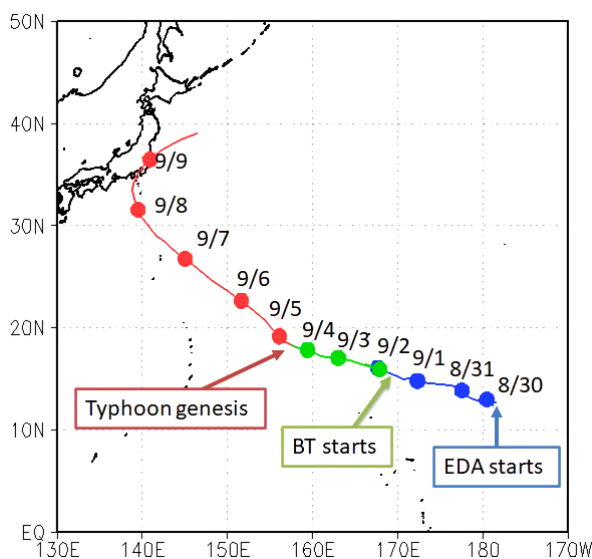


Fig. 1. Track (solid line) and daily locations at 00 UTC (circles) of Faxai in 2019 derived from the BT and EDA data. The blue line denotes the track detected only by the EDA, the green line denotes the track from the first detection of the BT data to typhoon genesis, and the red line denotes the track of the typhoon after it had reached tropical storm intensity.

odology and data. Section 3 describes the main environmental factors and contribution of the surrounding environment to Faxai's genesis. Section 4 discusses the contribution of the surrounding environment to Faxai's genesis compared with other cases. Finally, Section 5 summarizes the study.

2. Methodology and data

This study uses a modified version of the TGS by the JMA, which we hereafter refer to as JMA-TGS. Similar to the conventional TGS, the JMA-TGS calculates scores for five previously proposed environmental factors. As an example, the EW score is calculated as follows:

$$SCR_{EW} = A \cdot \left(\frac{\partial v}{\partial x} \right) \cdot \exp(B \cdot dist_{\min_EW}), \quad (1)$$

where v is the meridional wind at 850 hPa, and $dist_{\min_EW}$ is the distance between the nearest trough grid and the genesis location (hereafter, TGS location). We searched for a trough grid of the easterly wave, which was determined as the location where the meridional wind was northward to the east and southward to the west. A and B are arbitrary constants,

where $A = 2.0 \times 10^{-1}$ and $B = -1.0 \times 10^{-2}$. To determine the main contributor to Pre-Faxai, the five scores were normalized by their maximum and minimum values such that they were all between zero and one. The details are provided in Yoshida and Ishikawa (2013).

As an improvement on the conventional TGS, the JMA-TGS uses the location and time first detected by the EDA as the TGS location and time. Briegel and Frank (1997) showed that the occurrence of tropical disturbances was affected by large-scale flows for a period of about 3 days. For a conventional TGS time, the scores for the shear line, confluence region, monsoon gyre, and EW were obtained by analyzing data collected 66 h and 72 h before the first detection according to the BT data, while the score of Rossby wave energy dispersion from a preexisting TC was obtained from the first detection time. For the TGS time of JMA-TGS, scores for the four environmental factors were obtained using data collected 24, 48, and 72 h before the first detection according to the EDA (hereafter referred to as 24-h JMA-TGS and similar terms); the score of Rossby wave energy dispersion from a preexisting TC was obtained by the first detection time to the EDA (00-h JMA-TGS). The factor with the highest score was considered the main contributor to the occurrence of Pre-Faxai.

This study used the Grid-TGS developed by Yoshida and Fudeyasu (2020) to investigate the temporal and spatial changes in the environmental factors around Pre-Faxai. While the JMA-TGS was calculated for the genesis location of Faxai with reference to the BT data, the Grid-TGS was calculated on each grid point at each time for the input data in a similar manner to the JMA-TGS. For example, the grid score for EW is calculated as follows:

$$\text{Grid-SCR}_{\text{EW}} = \left(\frac{\partial v}{\partial x} \right) \cdot \exp(-1 \cdot \text{dist}_{\text{min_EW}}). \quad (2)$$

The details are provided in Yoshida and Fudeyasu (2020). Note that the Grid-TGS becomes high when the distance is short. Because each grid point of the input data is considered a candidate for the genesis location at each time in the calculation of the grid score, information reading a real genesis location is not required. The grid score gives a spatial distribution of the environmental conditions. For simplicity, the grid score is not normalized, and the grid score was not applied to determine the main contributor. The grid score used the Japanese 55-year Reanalysis Project (JRA55) (Kobayashi et al. 2015) as the input data. The JRA55 dataset has a horizontal resolution of 1.25° for

both longitude and latitude, with a 6-h time interval. To compare the grid score values, this study calculated the climatological mean of scores averaged over a 38-year period from 1979 to 2016.

The contributions of the surrounding environment to changes in the intensity of Pre-Faxai during Faxai's genesis stage were quantified using the TIFS, which is essentially a modified version of the statistical hurricane intensity prediction scheme (DeMaria and Kaplan 1994, 1999; DeMaria et al. 2005). It predicts the change in maximum wind speed of a typhoon, as well as the central pressure. Because the BT data include the TC central pressure before genesis, but not the maximum wind speed of a typhoon, the central pressures predicted by the TIFS at a forecast time of 6 h were compared to pressure derived from the BT data. The atmospheric data and central pressures at the initial time of each TIFS forecast in this study were derived from JRA55 and BT data. There are 26 predictors in the TIFS, which are predictors already used in the statistical hurricane intensity prediction scheme plus meteorological satellite image data (Shimada et al. 2018).

This study used merged infrared satellite images obtained by the Global Precipitation Measurement mission (Hou et al. 2014; Skofronick-Jackson et al. 2017). Merged data for the Global Precipitation Measurement multisatellite, including the Geostationary Meteorological Satellite, provide a blackbody temperature (T_{BB}) over the WNP and the ENP, with a temporal resolution of 30 min and spatial resolution as small as $0.1^\circ \times 0.1^\circ$.

3. Results

3.1 Environmental factors during the genesis stage of Faxai

Figure 2 shows the scores for the five environmental factors of the JMA-TGS, corresponding to the first detection of Pre-Faxai according to the EDA. With the exception of the score of the monsoon gyre for 48-h JMA-TGS, only the EW score exceeded zero. The score of the Rossby wave energy dispersion from a preexisting TC for 00-h JMA-TGS was zero because of the absence of a preexisting TC near Pre-Faxai. Therefore, the EW pattern was the environmental factor associated with the genesis of Pre-Faxai.

Figure 3 shows the distribution of the Grid-TGS score for EW (hereafter, Grid-EW) and the climatological mean for Grid-EW (Clim-Grid-EW). Grid-EW scores were averaged over the 3-day period from 12 UTC August 26 to 12 UTC August 29, 2019, before the first detection of Pre-Faxai by the EDA. The

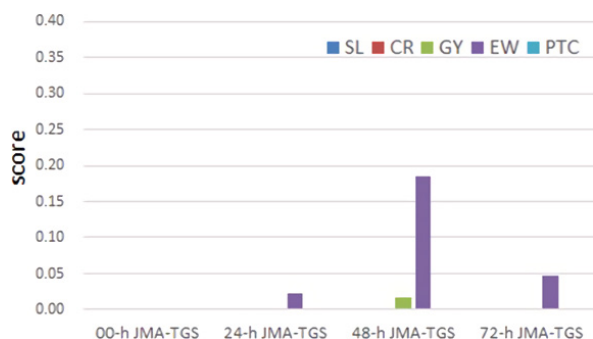


Fig. 2. Scores for the environmental factors of Faxai at the 00, 24, 48, and 72-h JMA-TGS time points, based on the time and position of Faxai at 12 UTC August 29, 2019, according to the EDA. SL, shear line; CR, confluence region; GY, monsoon gyre; PTC, Rossby wave energy dispersion from a preexisting TC.

Grid-EW extends east to west in a belt shape within 5–15°N in the North Pacific. Compared with Clim-Grid-EW averaged for the same period, the distribution of the Grid-EW scores was similar to that of the climatological mean, but the value of the Grid-EW score associated with Pre-Faxai was higher than that of Clim-Grid-EW. Figure 4 shows the time series of daily values for each Grid-EW score and the Clim-Grid-EW score, which were averaged over the region around Pre-Faxai bounded by 5–20°N and 160°E–160°W. Daily Clim-Grid-EW scores changed seasonally and reached a maximum in mid-August. The Grid-EW value around Pre-Faxai was approximately twice as large as Clim-Grid-EW with the second largest value in the past 38 years.

Figure 5 shows the horizontal winds and the relative vorticity at 850 hPa, as well as Grid-EW scores. The area with high Grid-EW scores (greater than 0.12) as-

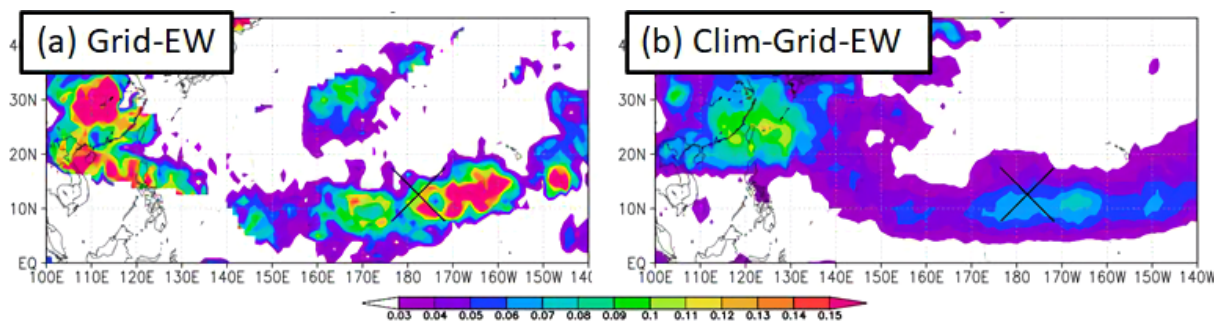


Fig. 3. The distribution of (a) Grid-EW averaged over the 3-day period from 12 UTC August 26 to 12 UTC August 29, 2019, and (b) Clim-Grid-EW averaged over the 3-day period from 12 UTC August 26 to 12 UTC August 29 from 1979 to 2016. Areas with values greater than 0.03 are shaded. The cross represents the position of Pre-Faxai at 12 UTC August 29, 2019.

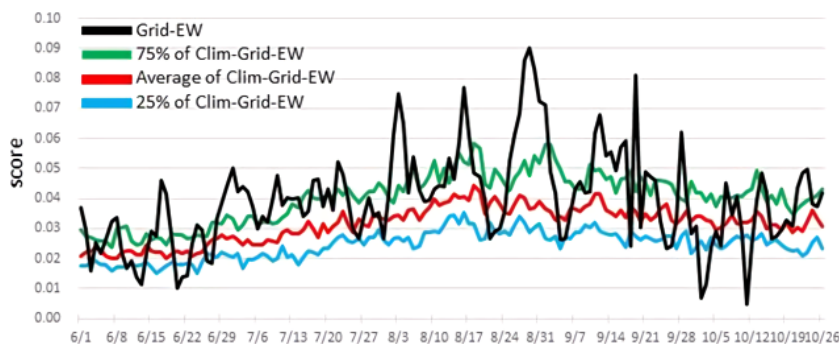


Fig. 4. Daily values of Grid-EW (black) in 2019, average of Clim-Grid-EW (red), 75 % confidence interval (green), and 25 % confidence interval (blue) of all cases of Grid-EW averaged over the region bounded by 5–20°N and 160°E–160°W.

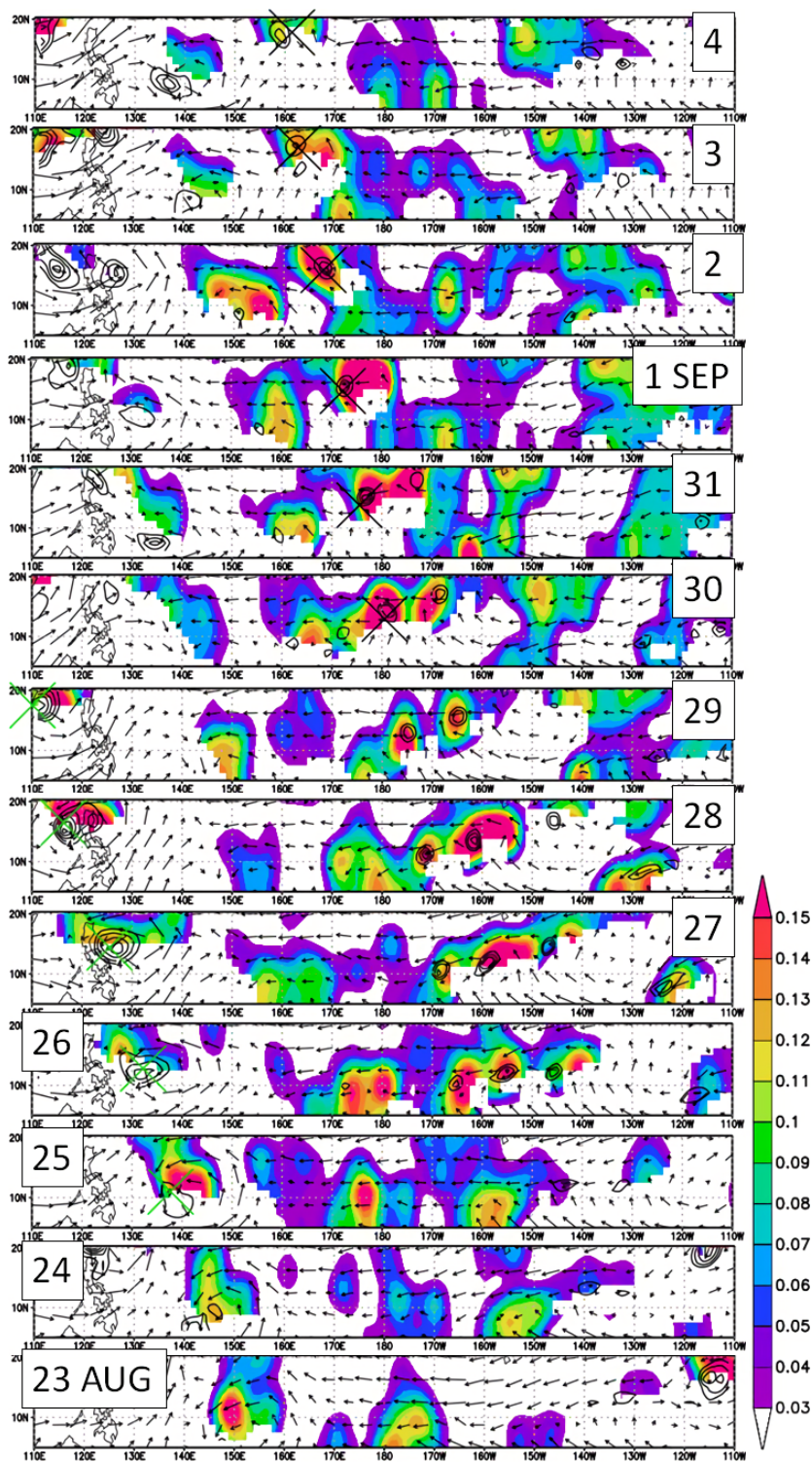


Fig. 5. Horizontal winds (m s^{-1} ; vectors) and relative vorticity (s^{-1} ; contour) at 850 hPa and Grid-EW values (shaded). The contour area indicates a relative vorticity greater than $4.0 \times 10^{-5} \text{ s}^{-1}$, and the contour interval is $2.0 \times 10^{-5} \text{ s}^{-1}$. Areas of Grid-EW values greater than 0.03 are shaded. The cross represents the position of Pre-Faxai (black) and Typhoon Podul (green).

sociated with Pre-Faxai could be traced to August 25, when it was around 158°W , 10°N . This suggested that the environmental preconditioning leading to the genesis stage of Faxai started over the ENP and moved westward to the WNP. The environmental conditions built up diabatically due to the convergence associated with the intertropical convergence zone in the ENP, which began to be restored on August 23.

Within the lower-troposphere environment characterized by high Grid-EW scores, three cyclonic vortices with a relative vorticity greater than $4.0 \times 10^{-5} \text{ s}^{-1}$ developed around 165°W (Pre-Faxai), 157°W , and 145°W on August 26. In infrared images derived from the Global Precipitation Measurement (Fig. 6), the clouds that developed into Pre-Faxai could be traced as band-like clouds on August 25. Although the origin of Pre-Faxai in the band-like clouds developed due to the horizontal shear in the lower troposphere (Fig. 5), an interval of 10 days was necessary for one of the vortices to develop into a typhoon, unlike previously studied conspicuous intertropical convergence zone breakdowns (Hack et al. 1989). Easterly waves represent a broad category of disturbances in the easterly wind environment in the tropics. They include large-scale traveling waves with respect to background flows (e.g., Serra et al. 2008), as well as wavy disturbances arising from baroclinic and barotropic instabilities, such as the well-known African EWs (e.g., Burpee 1972; Thorncroft et al. 2008). The disturbance associated with the present vortices could be regarded as an EW. Whereas its wavelength of $\sim 1000 \text{ km}$ was smaller, it is consistent with the results of a previous statistical study (Fudeyasu and Yoshida 2018).

The vortices moved westward at $5\text{--}6 \text{ m s}^{-1}$ because of the background easterly flow (Fig. 5), which was $4\text{--}8 \text{ m s}^{-1}$ between 950 hPa and 500 hPa (not shown). Figure 7 shows the 850-hPa streamlines under the co-moving frame for Pre-Faxai. The streamlines around the vortices that developed into Pre-Faxai were closed circulations under the co-moving frame. The closed circulation in the co-moving frame served to contain moisture and cyclonic vorticity, providing favorable conditions for tropical cyclogenesis (Dunkerton et al. 2009). This will be discussed in the next section.

The mid- and upper-troposphere cyclonic vortex, which was placed over the lower-troposphere vortex, could not be traced backward in time before August 29 (not shown), implying that the disturbance did not previously have a rigid vertical structure. Figure 8 shows the winds and geopotential heights at 200 hPa and the vertical wind shear between 850 hPa and 200 hPa. On August 26, a deep trough to the north extending to the

southwest was observed (Fig. 8a). On the south side of the trough, the vertical wind shear was enhanced by the westerly winds in the upper troposphere and the easterly winds in the lower troposphere. The strong vertical shear of more than 15 m s^{-1} would suppress the vortex developing into Pre-Faxai. Although the lower-troposphere environment associated with high Grid-EW scores was favorable for vortex formation, the strong vertical shear due to the deep trough slowed the development of the vortex over the ENP.

3.2 Contributions of the large-scale environment to the genesis of Faxai

According to the EDA and BT data, Pre-Faxai moved westward in the WNP during Faxai's genesis stage (Fig. 1). From the temporal changes in Grid-EW scores (Fig. 5), it was apparent that the area with high Grid-EW scores associated with Pre-Faxai continued to move westward and entered the WNP. This suggests that the lower-troposphere environment continued to be favorable for vortex formation over the WNP.

Figure 9 shows the time series of sea-level central pressure for Faxai from the BT data and the TIFS model at a forecast time of 6 h. Because the TIFS forecasts are determined by multiple linear regression, the accuracy of TIFS forecasts decreases with increasing forecast time. The accuracies of the changes in intensity up to a forecast time of 6 h, as predicted by TIFS, are generally high. This is an important consideration for statistical evaluation of the contributions of large-scale environmental conditions to the development of Pre-Faxai. According to the BT data, Pre-Faxai was first detected at 00 UTC September 2, 3.5 days after the first detection of Pre-Faxai by the EDA. No significant changes were found in Faxai's intensity up to 18 UTC September 3. The central pressure decreased gradually thereafter: typhoon genesis was observed at 18 UTC September 4. These trends in the central pressure change were captured by the TIFS forecasts: the mean decrease in central pressure from 12 UTC September 2 to 06 UTC September 4 (from 12 UTC September 4 to 00 UTC September 5) was $1.9 \text{ hPa (6 h)}^{-1}$ in the early genesis stage [$3.0 \text{ hPa (6 h)}^{-1}$ in the late genesis stage]. These data allowed evaluation of the contributions of large-scale environmental conditions to changes in the intensity of Pre-Faxai, although TIFS forecasts tend to over-forecast slightly in the early genesis stage.

As shown in Fig. 10, the magnitude of the central pressure decreased in Pre-Faxai with fractions for each TIFS predictor at a forecast time of 6 h, over interval of 6 h. The main predictors with a contribution

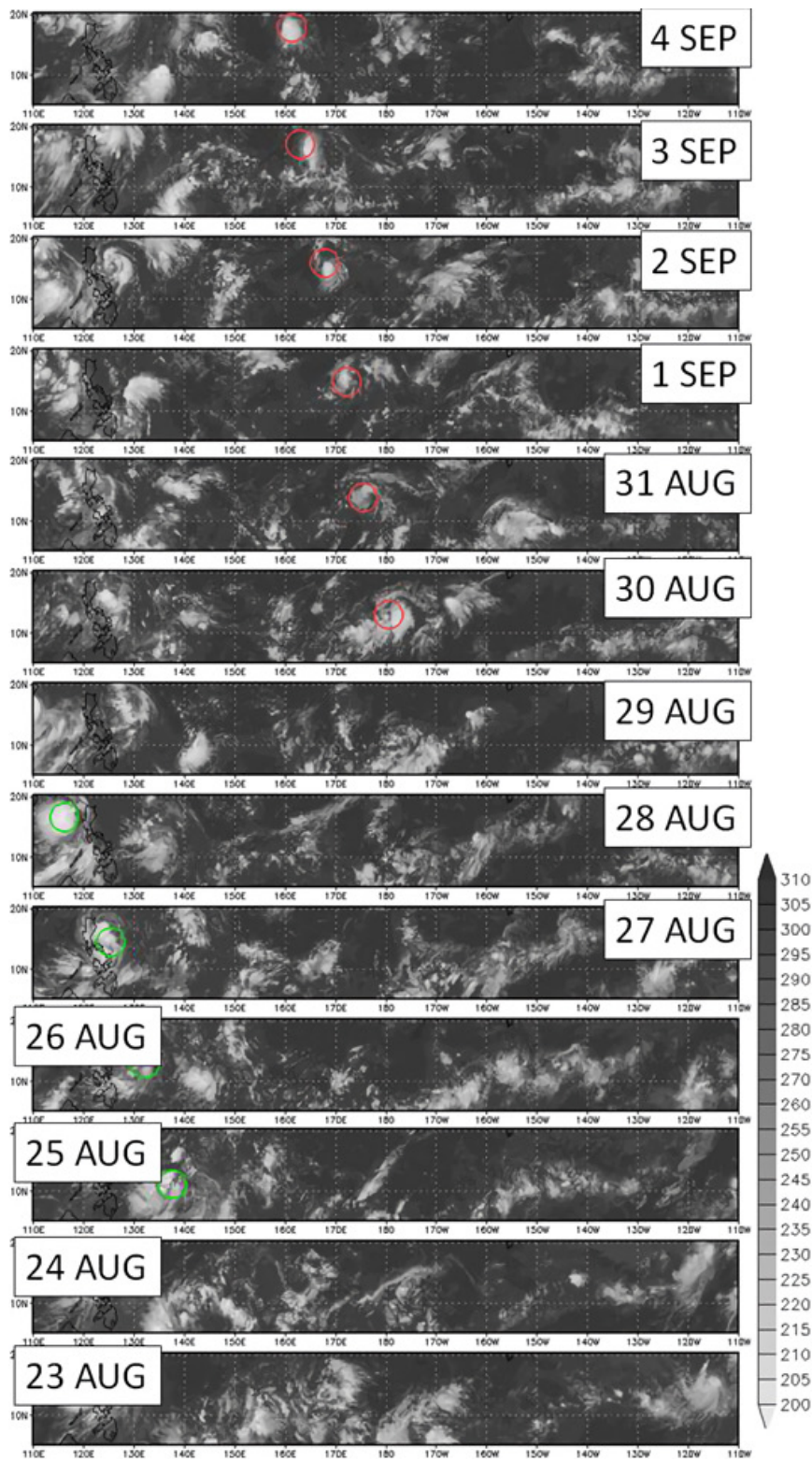


Fig. 6. The T_{BB} distribution from the infrared images obtained by the GPM mission. The circles represent the position of Pre-Faxai (red) and Typhoon Podul (green).

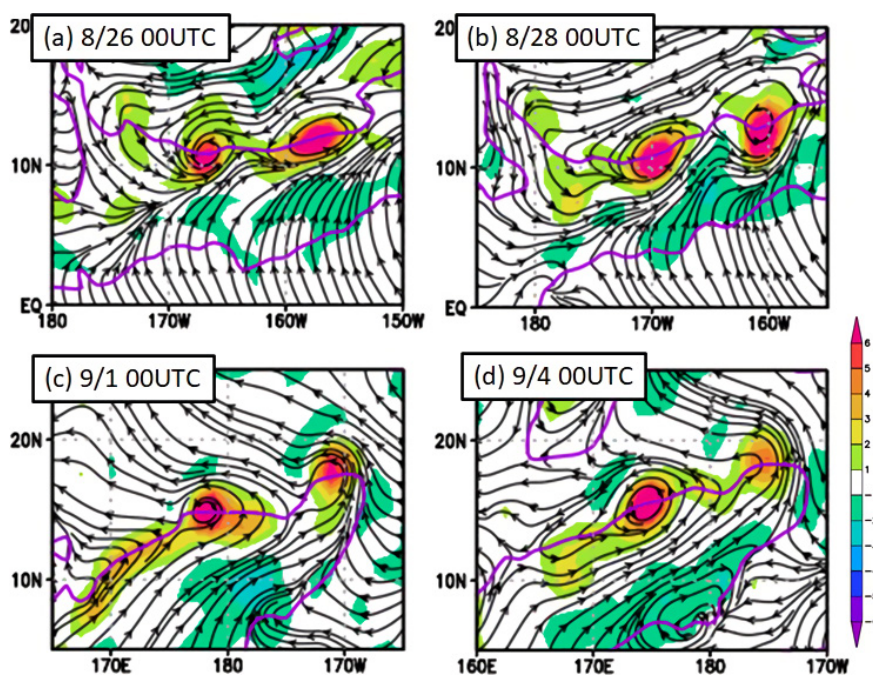


Fig. 7. The 850-hPa co-moving streamlines around Pre-Faxai at (a) 00 UTC August 26, (b) 00 UTC August 28, (c) 00 UTC September 1, and (d) 00 UTC September 4, 2019. Shading indicates a vertical relative vorticity (10^{-5} s^{-1}). Purple curves indicate zero relative zonal flow. The co-moving frame removes 5 m s^{-1} west–northwestward propagation speed. The relative vorticity is not impacted by the co-moving translation.

of a linear effects more than $1.0 \text{ hPa} (6 \text{ h})^{-1}$ were as follows: the difference between the maximum potential intensity (Emanuel 1986) and the maximum wind speed of a typhoon (POT), ocean heat content (OHC), and the magnitude of vertical wind shear (SHDC). Here, a positive value indicates a pressure decrease. With an average value of $+2.8 \text{ hPa} (6 \text{ h})^{-1}$, the predictor of POT related to the maximum potential intensity contributed to Pre-Faxai's intensity throughout the genesis stage. The averaged OHC was $+2.6 \text{ hPa} (6 \text{ h})^{-1}$ throughout the genesis stage, significantly contributing to the development of Pre-Faxai's intensity. The sea surface temperature and OHC in the central North Pacific during the genesis stage were both very high (sea surface temperature more than 30°C), and Pre-Faxai passed over this warm ocean (not shown). The SHDC had an average value of approximately $-1.1 \text{ hPa} (6 \text{ h})^{-1}$ in the early genesis stage from 12 UTC September 2 to 18 UTC September 3 and $+1.8 \text{ hPa} (6 \text{ h})^{-1}$ in the late genesis stage from 00 UTC to 18 UTC September 4. The change in the contribution of SHDC in the late genesis stage presumably promoted the development of Pre-Faxai.

At 12 UTC August 29, the time Pre-Faxai was first

detected by the EDA, a deep trough developed in the upper troposphere (Fig. 8b). On September 1, two upper cold lows were generated and separated from the upper-troposphere trough. In this study, an upper cold low is defined as a depression with a cold air center in the upper troposphere, and it is related to a cutoff low in either midlatitude westerlies (Molinari and Vollaro 1989; Postel and Hitchman 1999; Sakamoto and Takahashi 2005) or a tropical upper tropospheric trough cell (Sadler 1976; McTaggart-Cowan et al. 2013). Pre-Faxai moved westward, approaching one of the upper cold lows around September 3 (Fig. 8c). The TIFS showed that SHDC made a negative contribution to the development of Pre-Faxai (Fig. 10); the strong vertical shear south of this upper cold low continued to provide an unfavorable environment for the development of Pre-Faxai.

Figure 11 shows averaged infrared images derived from the Global Precipitation Measurement and the vertical wind shear between 200 hPa and 850 hPa during the genesis stage. The infrared images are averaged radially from the Pre-Faxai center to the 100-km radius. On September 1, clouds were distributed over a wide range under a weak vertical shear

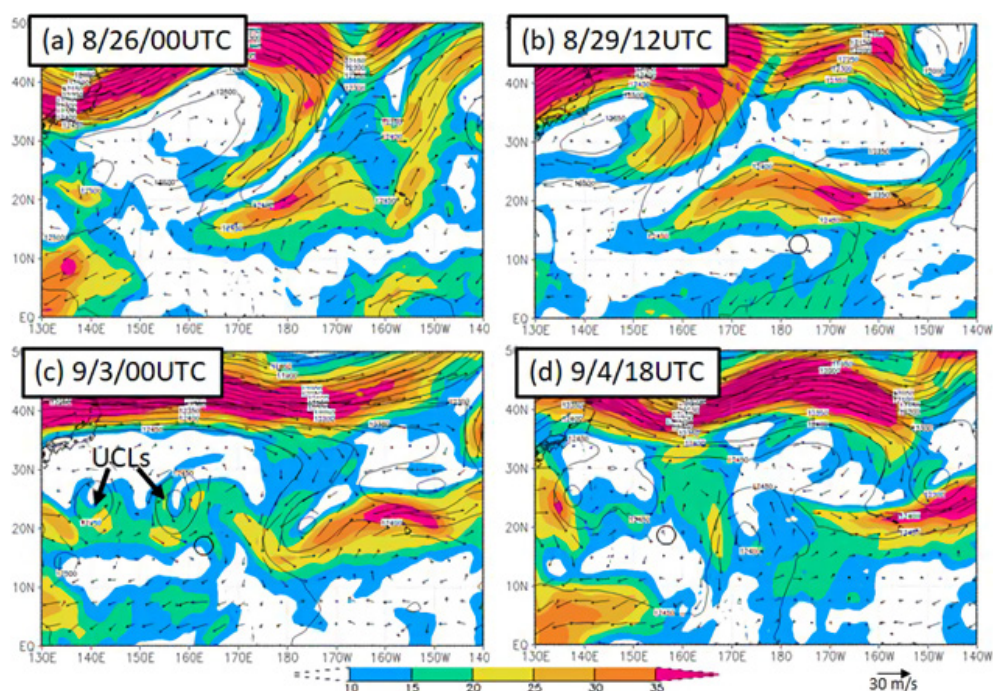


Fig. 8. Winds (m s^{-1} ; vectors), geopotential height (contours) at 200 hPa, and the magnitude of vertical wind shear between 850 hPa and 200 hPa (shaded) at (a) 00 UTC August 26, (b) 12 UTC August 29, (c) 00 UTC September 3, and (d) 18 UTC September 4, 2019. The regions with a magnitude of vertical wind shear greater than 10 m s^{-1} are shaded. The contour interval is 50 m. The black circle represents the position of Pre-Faxai.

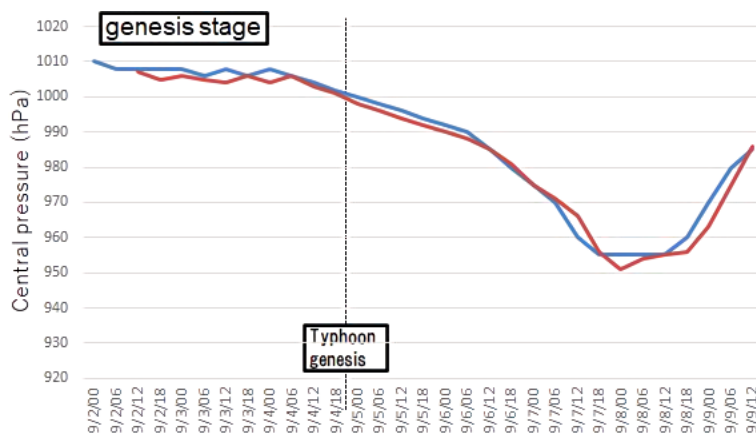


Fig. 9. Time series of sea-level central pressure for Faxai from the BT data (blue) and TIFS at a forecast time of 6 h (red).

environment. The clouds then developed more deeply within a 100-km radius of the Pre-Faxai center on September 2 under a strong westerly shear environment. They mainly distributed east of the center of Pre-Faxai ($0\text{--}180^\circ$). The cloud area was swept to the

eastern side. Although the environment characterized by the warm ocean provided favorable conditions for the development of Pre-Faxai, the strong vertical shear enhanced by the upper cold low presumably suppressed the deep clouds. At 18 UTC September

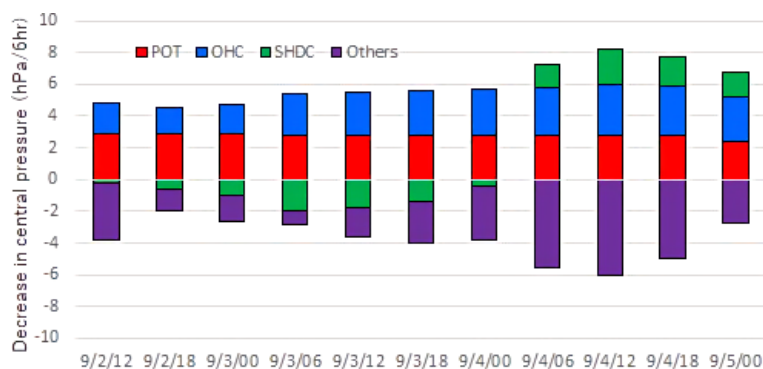


Fig. 10. Time series (6-h intervals) of the contribution of central pressure changes of Pre-Faxai, divided by three main predictors, derived from the TIFS at a forecast time of 6 h. Note that positive (negative) values indicate the development (decline) of Pre-Faxai's intensity.

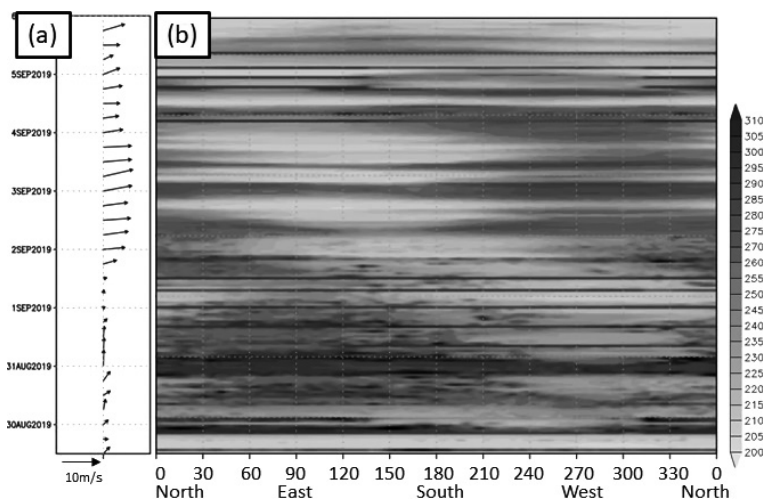


Fig. 11. (a) The vertical wind shear between 200 hPa and 850 hPa averaged within a 500-km radius of the TC center (arrows; scale at bottom left). (b) T_{BB} distribution (shaded; K) radially averaged along a 100-km radius from the TC center. Images are obtained from the Global Precipitation Measurement merged infrared.

4, westerlies in the upper troposphere decreased due to the weakening upper cold low (Fig. 8d), resulting in weak vertical shear around Pre-Faxai (Figs. 10, 11a). Clouds developed more deeply within a 100-km radius of the center of Pre-Faxai (Fig. 11b). Pre-Faxai developed and eventually reached tropical storm intensity, resulting in typhoon genesis.

4. Discussion

Our results using JMA-TGS showed that the initial vortex that developed into Pre-Faxai within the large-scale flow pattern was mainly associated with EWs over the North Pacific. Dunkerton et al. (2009)

estimated the center of a closed cyclone, which was termed a recirculating Kelvin cat's eye, based on the occurrence of tropical disturbances associated with EWs over the ENP and North Atlantic. The Kelvin cat's eye within the critical layer represents the optimal location for the occurrence of tropical disturbances because it provides a containment area. The area provides a containment effect inside the vortex for moisture, entrained by the developing circulation and/or lofted by the deep convection therein.

As shown in Fig. 7, the large-scale flows of high Grid-EW scores associated with Pre-Faxai consisted of vortices that moved due to the mean flow. The initial

vortex developed a closed circulation around them. A Kelvin cat's eye presumably developed, which satisfied the conditions suggested by Dunkerton et al. (2009). This is likely to be one of the reasons that the vortices persisted for long periods prior to dissipation.

Regarding the typhoon genesis of Faxai, the key environmental condition that resulted in the achievement of tropical storm intensity was a decrease in the vertical wind shear. In the early genesis period, an upper cold low was present to the northwest of Pre-Faxai, which inhibited the development of Pre-Faxai because of strong vertical wind shear (Figs. 10, 11). However, the favorable environment around Pre-Faxai throughout the genesis stage was characterized by a warm ocean and the strong vertical wind shear.

A statistical analysis (Fudeyasu and Yoshida 2019) of the genesis of TCs during the 38 years from 1979 to 2016 was performed to determine whether an upper cold low existed within the northwestern quadrant 1,500 km from the TC center, at the time of the first detection according to the BT data. In approximately 9 % of all TC cases, typhoon genesis was associated with an upper cold low, which provided favorable conditions for typhoon genesis because of upper-level divergence and convective available potential energy. When Pre-Faxai approached the upper cold low, the value of the TIFS predictor related to the upper-level divergence was $-0.1 \text{ hPa} (6 \text{ h})^{-1}$. This had a minimal effect on typhoon genesis. Pre-Faxai was generated in association with the large-scale flows of EWs, which dominated in the lower troposphere. Along with EWs in the lower troposphere, the vertical wind shear was enhanced by westerly winds in the upper troposphere caused by the upper cold low. Therefore, the upper cold low negatively contributed to the development of the TC. The contribution of upper cold lows to the development of Pre-Faxai may have differed according to environmental factors proposed by Ritchie and Holland (1999). Such contributions should be a research target for future studies.

5. Conclusion

This study investigated the contribution of the large-scale environment for the typhoon genesis of Faxai. Using the JMA-TGS, environmental factors proposed by Ritchie and Holland (1999) contributing to the occurrence of Pre-Faxai were revealed. In this regard, the large-scale flows of EWs were important. The Grid-EW score averaged for the time and the location where Pre-Faxai was first detected by the EDA was approximately twice as large as the climatological mean for Grid-EW, and it was the second largest value

in the past 38 years. The area with high Grid-EW scores that developed into Pre-Faxai can be traced back to 158°W on August 25, 2019.

The results of the TIFS forecast showed that the ocean conditions significantly contributed to the development of Pre-Faxai throughout the genesis stage, whereas strong vertical wind shear would suppress the development of Pre-Faxai. The vertical wind shear was enhanced by a combination of upper-troposphere westerly winds associated with an upper cold low and lower-troposphere easterly winds associated with EWs. In the late genesis period, the contribution of the vertical wind shear increased when the vertical wind shear decreased due to the weakening upper cold low. Pre-Faxai eventually reached tropical storm intensity. The key factors for typhoon genesis were the ocean conditions and the temporal changes in the vertical wind shear caused by the weakening upper cold low.

The organized clouds of Pre-Faxai in the area with high Grid-EW scores could be traced backward for an extended period from the ENP to the central North Pacific. There remains no specific explanation for the long genesis stage of Faxai. In addition, the mechanism of cloud organization leading to Pre-Faxai in the EW remains an open question. However, this study showed that the environmental factors associated with the genesis of Faxai formed over the ENP 10 days before typhoon genesis. These results imply that a tropical disturbance associated with EWs can be predicted over a long period before typhoon genesis. Monitoring the contributions of large-scale environmental conditions associated with initial tropical disturbances over the ENP through the Grid-TGS and TIFS is important for TC disaster prevention over the WNP.

Data Availability Statement

The BT can be derived from the JMA website available at <https://www.jma.go.jp/jma/jma-eng/jma-center/rsmc-hp-pub-eg/trackarchives.html>. The datasets of EDA and TIFS analyzed in this study are not publicly available.

Acknowledgments

The authors wish to thank the editor and two anonymous reviewers for their careful peer review, important comments, and useful suggestions that improved this article. This research was conducted in collaboration with the JMA and Meteorological Research Institute of JMA and utilized the dataset of JMA-TGS, EDA, TIFS, and JRA55 provided by the JMA. This work is supported by the Ministry of Education,

Culture, Sports, Science and Technology (MEXT) KAKENHI Grant 19K24677, 19H00705, 19H05696, and 21K03658. This work also is supported by the joint research program of CEReS, Chiba University (CJ20-23), and Integrated Research Program for Advancing Climate Models (TOUGOU program) from the MEXT, Japan.

Appendix: Abbreviations

Abbreviation	Definition
BT	The best-track data of the Regional Specialized Meteorological Center Tokyo–Typhoon Center
Clim-Grid-EW	The climatological mean for Grid-EW
EDA	Early Dvorak Analysis
ENP	The eastern North Pacific
EWs	Easterly waves
Grid-EW	Grid-TGS score for EW
JMA	Japan Meteorological Agency
JMA-TGS	A modified version of the TGS by the JMA
JRA55	The Japanese 55-year Reanalysis Project
OHC	Ocean heat content
Pre-Faxai	The tropical disturbance that developed to Typhoon Faxai
POD	The predictor related to the maximum potential intensity
SDHC	The magnitude of vertical wind shear
T_{BB}	A blackbody temperature
TGS	TC genesis score
TIFS	Typhoon Intensity Forecast Scheme
WNP	The western North Pacific

References

- Briegel, L. M., and W. M. Frank, 1997: Large-scale influences on tropical cyclogenesis in the western North Pacific. *Mon. Wea. Rev.*, **125**, 1397–1413.
- Burpee, R. W., 1972: The origin and structure of easterly waves in the lower troposphere of North Africa. *J. Atmos. Sci.*, **29**, 77–90.
- Chang, H.-R., and P. J. Webster, 1990: Energy accumulation and emanation at low latitudes. Part II: Nonlinear response to strong episodic equatorial forcing. *J. Atmos. Sci.*, **47**, 2624–2644.
- Chen, S. S., R. A. Houze, Jr., and B. E. Mapes, 1996: Multi-scale variability of deep convection in relation to large-scale circulation in TOGA COARE. *J. Atmos. Sci.*, **53**, 1380–1409.
- Chen, T.-C., and S.-P. Weng, 1998: Interannual variation of the summer synoptic-scale disturbance activity in the western tropical Pacific. *Mon. Wea. Rev.*, **126**, 1725–1733.
- DeMaria, M., and J. Kaplan, 1994: A Statistical Hurricane Intensity Prediction Scheme (SHIPS) for the Atlantic basin. *Wea. Forecasting*, **9**, 209–220.
- DeMaria, M., and J. Kaplan, 1999: An updated Statistical Hurricane Intensity Prediction Scheme (SHIPS) for the Atlantic and eastern North Pacific basins. *Wea. Forecasting*, **14**, 326–337.
- DeMaria, M., M. Mainelli, L. K. Shay, J. A. Knaff, and J. Kaplan, 2005: Further improvements to the Statistical Hurricane Intensity Prediction Scheme (SHIPS). *Wea. Forecasting*, **20**, 531–543.
- Dunkerton, T. J., M. T. Montgomery, and Z. Wang, 2009: Tropical cyclogenesis in a tropical wave critical layer: Easterly waves. *Atmos. Chem. Phys.*, **9**, 5587–5646.
- Dvorak, V. F., 1984: Tropical cyclone intensity analysis using satellite data. *NOAA Tech. Rep. NESDIS*, **11**, 47 pp. [Available at https://books.google.co.in/books?hl=en&lr=&id=59re76b5Bb1C&oi=fnd&pg=PR5&dq=%22Tropical+Cyclone+Intensity+Analysis+Using+Satellite+Data.+NOAA%22&ots=Nm2KdKoC3m&sig=ZcjrA72HTkexlH4rQAR-rTpuPpw&redir_esc=y#v=onepage&q=%22Tropical%20Cyclone%20Intensity%20Analysis%20Using%20Satellite%20Data.%20NOAA%22&f=false.]
- Emanuel, K. A., 1986: An air–sea interaction theory for tropical cyclones. Part I: Steady-state maintenance. *J. Atmos. Sci.*, **43**, 585–605.
- Fudeyasu, H., and R. Yoshida, 2018: Western North Pacific tropical cyclone characteristics stratified by genesis environment. *Mon. Wea. Rev.*, **146**, 435–446.
- Fudeyasu, H., and R. Yoshida, 2019: Statistical analysis of the relationship between upper tropospheric cold lows and tropical cyclone genesis over the western North Pacific. *J. Meteor. Soc. Japan*, **97**, 439–451.
- Fudeyasu, H., R. Yoshida, M. Yamaguchi, H. Eito, C. Muroi, S. Nishimura, K. Bessho, Y. Oikawa, and N. Koide, 2020: Development conditions for tropical storms over the western North Pacific stratified by large-scale flow patterns. *J. Meteor. Soc. Japan*, **98**, 61–72.
- Hack, J. J., W. H. Schubert, D. E. Stevens, and H.-C. Kuo, 1989: Response of the Hadley circulation to convective forcing in the ITCZ. *J. Atmos. Sci.*, **46**, 2957–2973.
- Heta, Y., 1990: An analysis of tropical wind fields in relation to typhoon formation over the western Pacific. *J. Meteor. Soc. Japan*, **68**, 65–77.

- Heta, Y., 1991: The origin of tropical disturbances in the equatorial Pacific. *J. Meteor. Soc. Japan*, **69**, 337–351.
- Hou, A. Y., R. K. Kakar, S. Neeck, A. A. Azarbarzin, C. D. Kummerow, M. Kojima, R. Oki, K. Nakamura, and T. Iguchi, 2014: The global precipitation measurement mission. *Bull. Amer. Meteor. Soc.*, **95**, 701–722.
- Kishimoto, K., 2009: *Revision of JMA's early stage Dvorak analysis and its use to analyze tropical cyclones in the early developing stage*. Technical Review, No. 10, RSMC Tokyo—Typhoon Center, 12 pp. [Available at <https://www.jma.go.jp/jma/jma-eng/jma-center/rsmc-hp-pub-eg/techrev/text10-1.pdf>.]
- Kishimoto, K., T. Nishigaki, S. Nishimura, and Y. Terasaka, 2007: *Comparative study on organized convective cloud systems detected through early stage Dvorak analysis and tropical cyclones in early developing stage in the western North Pacific and the South China Sea*. Technical Review, No. 9, RSMC Tokyo—Typhoon Center, 14 pp. [Available at <https://www.jma.go.jp/jma/jma-eng/jma-center/rsmc-hp-pub-eg/techrev/text9-2.pdf>.]
- Kobayashi, S., Y. Ota, Y. Harada, A. Ebata, M. Moriya, H. Onoda, K. Onogi, H. Kamahori, C. Kobayashi, H. Endo, K. Miyaoka, and K. Takahashi, 2015: The JRA-55 Reanalysis: General specifications and basic characteristics. *J. Meteor. Soc. Japan*, **93**, 5–48.
- Lander, M. A., 1994: Description of a monsoon gyre and its effects on the tropical cyclones in the western North Pacific during August 1991. *Wea. Forecasting*, **9**, 640–654.
- Li, T., and B. Fu, 2006: Tropical cyclogenesis associated with Rossby wave energy dispersion of a preexisting typhoon. Part I: Satellite data analyses. *J. Atmos. Sci.*, **63**, 1377–1389.
- Li, T., X. Ge, B. Wang, and Y. Zhu, 2006: Tropical cyclogenesis associated with Rossby wave energy dispersion of a preexisting typhoon. Part II: Numerical simulations. *J. Atmos. Sci.*, **63**, 1390–1409.
- McDonald, N. R., 1998: The decay of cyclonic eddies by Rossby wave radiation. *J. Fluid Mech.*, **361**, 237–252.
- McTaggart-Cowan, R., T. J. Galarnau, Jr., L. F. Bosart, R. W. Moore, and O. Martius, 2013: A global climatology of baroclinically influenced tropical cyclogenesis. *Mon. Wea. Rev.*, **141**, 1963–1989.
- Molinari, J., and D. Vollaro, 1989: External influences on hurricane intensity. Part I: Outflow layer eddy angular momentum fluxes. *J. Atmos. Sci.*, **46**, 1093–1105.
- Postel, G. A., and M. H. Hitchman, 1999: A climatology of Rossby wave breaking along the subtropical tropopause. *J. Atmos. Sci.*, **56**, 359–373.
- Ritchie, E. A., and G. J. Holland, 1999: Large-scale patterns associated with tropical cyclogenesis in the western Pacific. *Mon. Wea. Rev.*, **127**, 2027–2043.
- Sadler, J. C., 1976: A role of the tropical upper tropospheric trough in early season typhoon development. *Mon. Wea. Rev.*, **104**, 1266–1278.
- Sakamoto, K., and M. Takahashi, 2005: Cut off and weakening processes of an upper cold low. *J. Meteor. Soc. Japan*, **83**, 817–834.
- Serra, Y. L., G. N. Kiladis, and M. F. Cronin, 2008: Horizontal and vertical structure of easterly waves in the Pacific ITCZ. *J. Atmos. Sci.*, **65**, 1266–1284.
- Shimada, U., H. Owada, M. Yamaguchi, T. Iriguchi, M. Sawada, K. Aonashi, M. DeMaria, and K. D. Musgrave, 2018: Further improvements to the Statistical Hurricane Intensity Prediction Scheme using tropical cyclone rainfall and structural features. *Wea. Forecasting*, **33**, 1587–1603.
- Skofronick-Jackson, G., W. A. Petersen, W. Berg, C. Kidd, E. F. Stocker, D. B. Kirschbaum, R. Kakar, S. A. Braun, G. J. Huffman, T. Iguchi, P. E. Kirstetter, C. Kummerow, R. Meneghini, R. Oki, W. S. Olson, Y. N. Takayabu, K. Furukawa, and T. Wilheit, 2017: The Global Precipitation Measurement (GPM) mission for science and society. *Bull. Amer. Meteor. Soc.*, **98**, 1679–1695.
- Thorncroft, C. D., N. M. J. Hall, and G. N. Kiladis, 2008: Three-dimensional structure and dynamics of African easterly waves. Part III: Genesis. *J. Atmos. Sci.*, **65**, 3596–3607.
- Tsuchiya, A., T. Mikawa, and A. Kikuchi, 2001: Method of distinguishing between early stage cloud systems that develop into tropical storms and ones that do not. *Geophys. Mag.*, **4**, 49–59.
- Yamaguchi, M., H. Owada, U. Shimada, M. Sawada, T. Iriguchi, K. D. Musgrave, and M. DeMaria, 2018: Tropical cyclone intensity prediction in the western North Pacific basin using SHIPS and JMA/GSM. *SOLA*, **14**, 138–143.
- Yoshida, R., and H. Ishikawa, 2013: Environmental factors contributing to tropical cyclone genesis over the western North Pacific. *Mon. Wea. Rev.*, **141**, 451–467.
- Yoshida, R., and H. Fudeyasu, 2020: How significant are low-level flow patterns in tropical cyclone genesis over the western North Pacific? *Mon. Wea. Rev.*, **148**, 559–576.
- Zhang, C., and P. J. Webster, 1989: Effects of zonal flows on equatorially trapped waves. *J. Atmos. Sci.*, **46**, 3632–3652.